REPORT DOCUMENTATION PAGE

Public reporting burden for this collection of information is estimated to average 1 hour per response, including the time for reviewin gathering and maintaining the data needed, and completing and reviewing the collection of information. Send comments regarding t of information, including suggestions for reducing this burden to Washington Headquarters Service, Directorate for Information Ope 1215 Jefferson Davis Highway, Suite 1204, Arlington, VA 22202-4302, and to the Office of Management and Budget, Paperwork Reduction Project (0704-0188) Washington, DC 20503.

AFRL-SR-AR-TR-08-0182

PLEASE DO NOT RETURN YOUR FORM TO THE ABOVE ADDRESS.

1. REPORT DATE *(DD-MM-YYYY)*	2. REPORT TYPE	3. DATES COVERED (From - To)
	Final Technical Report	15 May 2007 – 30 November 2007

4. TITLE AND SUBTITLE
Nanojets: Electrification, Energetics, Dynamics, Stability and Breakup

5a. CONTRACT NUMBER

5b. GRANT NUMBER
FA9550-07-1-0420

5c. PROGRAM ELEMENT NUMBER

6. AUTHOR(S)
Dr. Uzi Landman

5d. PROJECT NUMBER

5e. TASK NUMBER

5f. WORK UNIT NUMBER

7. PERFORMING ORGANIZATION NAME(S) AND ADDRESS(ES)
School of Physics
Georgia Tech Research Corporation
Atlanta GA 30332-0430

8. PERFORMING ORGANIZATION REPORT NUMBER

9. SPONSORING/MONITORING AGENCY NAME(S) AND ADDRESS(ES)
USAF/AFRL
AFOSR
875 North Randolph Street
Arlington VA 22203
Dr Michael Berman/NA

10. SPONSOR/MONITOR'S ACRONYM(S)
AFOSR

11. SPONSORING/MONITORING AGENCY REPORT NUMBER
N/A

12. DISTRIBUTION AVAILABILITY STATEMENT

Distribution Statement A: Approved for public release. Distribution is unlimited.

13. SUPPLEMENTARY NOTES

14. ABSTRACT

The research during this 6 month grant was devoted to finalizing our work on the effect of electric fields on dielectric nanodroplets, as may be found during the breakup of electrified nanojets and colloidal thrusters. In our extensive molecular dynamics simulation, preformed for a 10nm droplet made of formamide molecules, the response of the nano-droplet to uniform electric fields was explored.

15. SUBJECT TERMS

16. SECURITY CLASSIFICATION OF:			17. LIMITATION OF ABSTRACT	18. NUMBER OF PAGES	19a. NAME OF RESPONSIBLE PERSON
a. REPORT	b. ABSTRACT	c. THIS PAGE			19b. TELEPONE NUMBER *(Include area code)*
Unclassified	Unclassified	Unclassified	Unclassified	52	(703)

FINAL REPORT

Nanojets: Electrification, Energetics, Dynamics, Stability and Breakup

Contract/Grant #: FA9550-07-1-0420

Reporting Period: 5/15/07-11/30/07

Prepared by:

Uzi Landman

School of physics

Georgia Institute of Technology

Atlanta, GA 30332-0430

Uzi. Landman@physics.gatech.edu

20080404131

I. Summary

The research during this 6 month grant was devoted to finalizing our work on the effect of electric fields on dielectric nanodroplets, as may be found during the breakup of electrified nanojets and colloidal thrusters. In our extensive molecular dynamics simulations, preformed for a 10nm droplet made of formamide molecules, the response of the nano-droplet to uniform electric fields was explored. Increasing fields were found to cause the initially spherical droplet to undergo gradual slight ellipsoidal deformation that culminated in a shape instability and a first-order shape transition to a slender needle at ~ 0.55 V/nm. For larger fields enhanced dipole ordering that leads to a first-order electro-crystallization transition was found, portrayed in sharp changes the molecular diffusion constant and in a positional order parameter. Both transitions were found to exhibit hysteresis upon decreasing the electric field. A dielectric continuum model was developed and tested against the results of the molecular dynamics simulations, resulting in good agreement.

.

Detailed descriptions of the molecular dynamics simulations, the analytical continuum model, and our analysis are given in section IV, titled:

Dielectric Nanodroplets: Structure, Stability, Thermodynamics, Shape Transitions and Electrocrystallization in Applied Electric Fields

II. Archival Publications

1. "Shape Transformation and Electrocrystallization of Polar Liquid Drops", W.D.

Luedtke, J. Gao and U. Landman, Phys. Rev. Lett. (2008).

2. " Dielectric Nanodroplets: Structure, Stability, Thermodynamics, Shape Transitions and Electrocrystallization in Applied Electric Fields", W.D.Luedtke, J. Gao and U. Landman, Phys. Rev. B (2008).

III. Researchers Supported by the Grant

1. Dr. Uzi Landman, Professor and Principal Investigator.
2. Dr. David Luedtke, Senior Research Scientist.
3. Dr. Jianping Gao, Senior Research Scientist

VI. Dielectric Nanodroplets: Structure, Stability, Thermodynamics, Shape Transitions and Electrocrystallization in Applied Electric Fields

The following is a manuscript prepared for publication by W. D. Luedtke, Jianping Gao and Uzi Landman

The response of a dielectric 10nm in diameter nano-droplet made of formamide to uniform electric fields is explored with molecular dynamics simulations. Increasing fields causes the initially spherical droplet to undergo gradual slight ellipsoidal deformation that culminates in a shape instability and a first-order shape transition at ~ 0.55 V/nm to a slender needle. For larger fields we find enhanced dipole ordering that leads to a first-order electro-crystallization transition, portrayed in sharp changes the molecular diffusion constant and in a positional order parameter. Both transitions exhibit hysteresis upon decreasing the electric field. A dielectric continuum model is developed

and tested against the results of the molecular dynamics simulations, resulting in good agreement.

I. INTRODUCTION

Neutral and charged dielectric drops of macroscopic dimensions and their response to applied uniform electric fields have been a subject of continued basic and applied research interest. A dielectric drop placed in an electric field is polarized and the balance between the electrical forces on the induced surface charges and the forces originating from capillary surface tension determines the shape the drop. Alternatively, this can be stated as a complex minimization problem searching for the shape that yields the lowest total energy (the sum of the electrical and surface contributions). The difficulty lies in the interdependence of the electric field distribution (as well as the surface tension or surface energy) and the shape, which must be determined self-consistently. This competition between electrical and capillary contributions emerges in many areas involving electrohydrodynamic flow. For example, some of the most relevant physics involved in colloid thrusters and electrospray devices operating in the cone-jet mode may be seen already in the simpler problem of an elongated liquid drop in a uniform external electric field, including the formation of electrified jets and emission and acceleration of small charged droplets at the ends of the elongated parent drops. This is a classic problem in the study of electrified fluids that has been studied both experimentally and theoretically [R12,23-24,31,33,38] and parallels similar phenomena in ferromagnetic fluid drops under the influence of an externally applied magnetic field (R12,23,38). Devices producing and utilizing drops are rapidly approaching nanometer scales and it is important to identify and understand the new phenomena that may emerge in the

electrohydrodynamics of fluid flow at these length scales, particularly those pertaining to the formation and stability of nano-scale droplets.

Here we focus on a molecular fluid, formamide $HCONH_2$ chosen because of it's high molecular electric dipole moment (3.7 D, that is twice that of an H_2O molecule) and the consequent propensity for solvation of salts at relatively high concentrations, thus making it a working material in current experimental, and theoretical, studies of investigations of electrosprays, electrified jets and colloidal thrusters [R10-11,13]. We note that formamide has also been the focus of experimental and theoretical studies since it represents a simple model compound displaying the same type of hydrogen bonding between amide groups present in many biological systems.

We perform a systematic study of a 10 nm diameter formamide droplet placed in a constant uniform electric field along a given axis (the z-axis). The field strengths we use are on the order of 1 V/nm, a value that is of relevance to current research in areas related to the formation and stability of droplets in electrosprays and colloid thrusters (ref. R11). This magnitude of the field is large enough to generate a pronounced elongation of the formamide droplet. We vary the field strengths over a wide range and compare the results obtained for these nano-scale dielectric drops to published continuum theory predictions (ref. R12,R23,R24,R3). Our results indicate that under the influence of fields of about 1.0-1.5 V/nm these drops will exhibit shape changes, transforming from equilibrium spheres at zero field to ellipsoidal shapes with long axis (c) to-short axis (a) ratios, $\lambda = c/a$, of the order of ~15-20. Furthermore, we find that for larger external electric fields first-order electro-crystallization of the drop occurs..

Namely the external field modifies the thermodynamics and phase behavior of a dielectric droplet.

It if of interest to note that electric field strengths of V/nm are ubiquitous in the study of fluid/vacuum interfaces involving charged and dielectric fluids under the influence of electric fields. In electrospray devices the electric fields at the apex of a Taylor cone [R23], where a fine jet is formed, is on the order of V/nm, even though the average field due the nozzle/extractor potential may be much smaller. This is true as well in the high curvature regions of droplets of dielectric/ionic mixtures in electric fields that are large enough to cause elongation and possible emission of charged droplets. Even under external field-free conditions, a charged droplet may fission or emit cluster ions when the excess charge is large enough (ref. R19), due to it's self-field, and under such circumstances the maximum field at the surface can again be of V/nm magnitude at the regions where much of the interesting and relevant physics takes place, e.g. where instabilities and charged jets emanate and clusters detach.

II. COMPUTATIONAL METHODOLOGY

The principal theoretical methodology employed by us is molecular dynamics (MD) simulations where the equations of motions of the interacting particles are solved numerically with very high spatial and temporal resolution (typically 0.01 nm and under 0.01 ps. To simulate systems that are large enough, thus allowing assessment of concepts derived on the basis of continuum theories, it is important to utilize simple efficient representations of the interatomic forces. Formamide is a planar molecule whose internal

degrees of freedom and intramolecular forces are of minor significance for the phenomena in which we are interested here. Consequently, we treat the formamide molecule as a solid body using quaternion dynamics (ref. R1), implemented via a mid-step implicit leap-frog algorithm (ref. R2) that has been shown to be an extremely stable integration scheme (with only a very small energy drift occurring for long simulation periods). The geometry of the molecule is taken from high-resolution X-ray studies of crystalline formamide (ref. R3).

In our simulations we employed the AMBER force field parameters (refs. R4-5) for the intermolecular van der Waals interactions between the atomic sites located on different molecules. For the atoms of the formamide molecule we use the CHELP-BOW (ref. R6) partial charges; these have been shown to give a good overall description of the electrostatic potential of the molecules. The weak inter-molecular van der Waals interactions are truncated on a group basis through the use of a smooth switching function (ref. R7) that depends on the distance between molecular centers of mass so that entire groups of atoms on one molecule interact with the entire group of atoms on another molecule, and dipole interactions are not truncated.

Since there have been few large-scale atomistic simulation involving electrohydrodynamics of complex fluids, we looked to simple initial studies to learn what issues are important in faithfully modeling such systems. In particular, we first explored using long-range Coulombic interatomic potentials with finite interaction cutoffs as this was a simple first approach that is sufficient in many simulations. However when we performed test studies of formamide droplets in uniform external electric fields of varying strengths, we noted significant cooperative effects within the dipolar fluid that

emerged as the cutoffs were increased from values of ~ 0.9 – 1.2 nm (typical values in many studies involving atomic partial charges) to 3.6 nm. Droplets (which when studied with small interaction cutoffs remain spherical) elongate as the cutoff is increased due to cooperative dipole-dipole and dipole-field interactions, in qualitative agreement with existing continuum theories of dielectric fluids in electric fields (refs. R12, R23-24). From these observations it became apparent that the long-range interactions needed to be treated more accurately (i.e., with no interaction range cutoffs).

To address these issues we implemented a parallel version of the *fast multipole method*, FMM, (ref. R8), tailored for our purposes. In the FMM a system is spatially represented in a large roughly cubic "root-cell". The latter contains a hierarchy, or "tree-structure" division, of "child" sub-cells obtained by dividing the root-cell into octants and then allowing these child cells to be the parent cells of further binary subdivisions until one reaches the smallest "leaf" cell. Electric multipole moments are computed for all cells at all levels from the atomic charges belonging to molecules contained within the cells. Atoms belonging to molecules in the basic leaf cell interact directly with all the atoms of molecules in neighboring leaf cells, while they interact only with the multipole moments of more remote cells; the more remote the cells are from the central leaf cell, the larger the cells are allowed to be. Thus an atom interacts with a small set of multipoles representing entire, increasingly larger, volumes of remote space, rather than with all of the atoms contained within it - this is the main feature that makes it possible to efficiently model large systems involving long-range interactions. We carried the multipole calculations to m=6 (m=0 and 1 are the monopole and dipole levels). The size

of the smallest, leaf, cell was 1.2 nm and this value was used as the spherical cutoff for the short range van der Waals interactions.

For the simulations performed at constant temperature, we use a velocity rescaling algorithm due to Berendsen et. al (ref. R41, also see ref. R1, Eq. 7.59) with a relaxation time of 3 ps. This is applied only to the molecular center of mass velocities. We have observed that equipartition of energy between translational and rotational degrees of freedom is very rapid and there is no need to directly modify the rotational kinetic energies. Additional details of our code necessary for this study will be described further as we discuss our results.

III. PROPERTIES OF THE FIELD – FREE LIQUID

To ascertain the faithfulness of the parametrized interaction potentials used in our simulations we tested first certain thermodynamic and physical properties of the simulated model, including evaluations of the melting point, surface tension, diffusion constant, and dielectric constant. Since experiments on liquid formamide are commonly performed at room temperature (that is about 25K above the melting point of crystalline formamide), we focus here on results obtained from room temperature MD simulations.

Melting point, density, diffusion constant and surface tension

The melting point of the modeled liquid formamide was estimated as the coexistence temperature of the crystalline and liquid phases. A crystalline slab containing ~5200 molecules in which there were two free surfaces (vacuum interfaces) along the z-axis, was constructed, with two-dimensional periodic boundary conditions (2D pbc's)

imposed in the x-y plane and reflecting boundary conditions whenever a gas phase molecule encounters the ends of the computational cell. In these simualtions we replicated the basic root-cell and "stacked" three of them along the z-axis to create a long narrow tree-structure (requiring an appropriately modified non-standard FMM algorithm: this is particularly useful for efficient simulations of systems such as highly elongated droplets and long liquid jets). The size of each FMM root-cell was ~5.8 nm (in the x direction), 4.7 nm (in y) and by 5.6 nm (in z) giving a z-dimension of the calculational cell of ~3×5.6nm ~ 16.8 nm, while the solid slab, centered about z=0, occupied ~11 nm along z, leaving ~3 nm of free space at each end of the computational cell. After equilibrating the system well below the experimental melting point, the energy of the system was elevated via scaling of the particles' velocities with subsequent lengthy constant energy equilibrations, until approximately 1/3 of the system was melted and continued to evolve in equilibrium with the remaining solid part. This point of liquid/solid coexistence point, i.e. the melting point, was found to be close to 285K, which is 9 K above the experimental value of 276K (ref R21). Since our plan was to perform our electrical field studies at room temperature, we chose to adjust the temperature of these simulations to a somewhat higher temperature (310 K) to account for the higher melting temperature of the simulated mode compared to experiment, and to assure that we are well into the temperature range corresponding to a liquid phase; the temperature difference between 300K and 310K is not expected to effect the physical behaviour of our system in any noticeable manner. The density of the crystal was found in our simulations to be 1.26 g/cm^3 in agreement with the experimental value (1.26 g/cm^3) (ref. R39).

The density and diffusion constant of liquid formamide were determined by us from constant (zero) pressure simulations of bulk liquid formamide, where the spatial dimensions of a cubical root-cell were allowed to vary, while using 3D pbc and the FMM using a modified constant-pressure algorithm (ref. R41, R1). We have also modified the FMM algorithm so that when employing pbc the tree-structure of the root-cell, along with all its computed multipoles, are replicated as neighboring image cells. In this way atoms in the central computational cell are acted on by the correct multipole structure as they interact with all of their neighboring periodic image cells. The width of the cubical root cell was ~6 nm. The density of the pure formamide liquid (at 310K) was found to be ~1.10 g/cm^3 in good agreement with the experimental value of 1.13 g/cm^3 (R21) and the computed diffusion constant was found to be ~1.2 $\times$ 10^{-5} cm^2/sec which compares well with values ranging from 0.55 to 1.27 $\times$ 10^{-5} cm^2/sec estimated from previous experiments and simulations (ref R40).

Since capillary forces are a major driving force in the phenomena that we study, it is important to obtain an estimate for the surface tension of the simulated liquid. To this aim we determined the surface tension of liquid formamide in two different ways. First, we simulated a liquid slab maintained at 310K with the same number of molecules and type of boundary conditions as in the liquid-solid coexistence study described above. In this case we replicate the basic root-cell three times along the z-axis. The width of each cubical FMM root-cell was ~5.6 nm giving a z-dimension of the calculational cell of 3×5.6~ 17nm, while the liquid slab, centered about z=0, occupied ~11 nm along z, leaving sufficient space to establish both liquid and vapor regions.

The normal (P_N) and tangential (P_T) components of the molecular pressure tensors were used to find the surface tension γ by integrating (P_N - P_T) across each liquid interface (ref. R20). The value that we found γ = 0.046 N/m compares with the experimentally determined value of γ_{exp} = 0.057 (ref R21).

In an alternative method, we used the fact that the pressure inside a spherical droplet of radius R is P = $2\gamma/R$. We formed a spherical drop of formamide by 'carving out' a ~10 nm diameter drop from the bulk constant pressure simulation system that we described earlier, and allowed it to equilibrate further using 'absorbing' boundary conditions; namely, the pbc were lifted and the few evaporating molecules that crossed the boundaries of the 19.2 nm wide FMM root cell were removed from the system. Using the averaged hydrostatic pressure in the interior of the drop and the drop's equimolar radius, we computed a value of γ = 0.046 N/m in agreement with our previous estimate. The density in the interior of the drop interior was found to be about 1.11 g/cm3; results obtained from simulations of a larger diameter drop (20 nm) agree well with these values).

IV. FIELD-INDUCED SHAPE AND CRYSTALLIZATION TRANSITIONS

In this section we focus on the thermodynamic and electric-field induced structural transformations of the dielectric nanodroplet, with the strength of the externally applied electric field serving as a control parameter. Our investigations were carried out at T=310K (see earlier discussion) and involved a droplet with a diameter of 10 nm; the droplet contains 7150 formamide molecules (that is, 6 x 7150 ~ 43000 atoms carrying partial charges). The properties of the drop as a function of the strength of the applied

electric field (from 0 to 3 V/nm) were determined from simulations where for each successively incremented value of the field the drop was fully equilibrated before equilibrium averaged results were computed.

Prior to presentation of our results we remark on certain aspects of the analysis of the MD results. Shape deformations of liquid drops induced by uniform external electric fields leading to the appearance of structures with geometries close to prolate spheroids , have been described experimentally and theoretically (using continuum pictures) (refs. R23, R24). Furthermore, under certain circumstances the emergence of conical regions near the ends of the elongated structures has been observed. In the present study we have found that the shape of a 10 nm formamide drop placed in a uniform electric field may indeed be well characterized as a prolate spheroid (with the aspect ratio $\lambda = c/a$ between the semi-major (long) and semi-minor (short) axes, varying as a function of the field strength), with some deviation emerging near the ends for sufficiently strong fields (i.e., for highly elongated spheroidal shapes). A prolate spheroid (ellipsoid) is described by the equation $(r_z/a)^2 + (z/c)^2 = 1$, and plots of r_z^2 vs z^2 from our simulation data exhibit a highly linear relationship; the minor and major axes and the corresponding aspect ratios, λ, are determined from least square fits to the above equation for different values of the applied field.

In finding the axial profile (r_z vs. z), the z-axis (along which the external electric field is applied and the droplet elongates) is divided into bins of width $dz = 0.2$ nm and the number of molecules N_Z in each bin is computed. Using the mean density, ρ, inside the droplet, an equimolar radius r_z is computed for each z-bin with the relation $\rho\pi r_z^2 dz = N_z$. Additionally, for the chosen bin width dz, one can determine a cutoff radius

r_c that corresponds to one molecule, N_z=1. This provides a natural cutoff for determining the size of the droplet, and in performing the least square fit of the averaged profile data to a prolate spheroid, contributions are included only from points within the cutoff radius; this procedure yields prolate spheroid shapes are consistent with the droplet profiles for both small and large elongations.

The density ρ inside a droplet is determined for each field strength by time averaging the density inside a test volume located in the interior of the droplet and having the representative shape of the droplet shape. This is done by making first a rough estimate of the semi-minor and semi-major axes using radial as well as axial binning of the atomic positions and determining the largest non-empty radial and axial bins respectively. The internal prolate spheroid test volume is defined by scaling the so determined lengths of the axes by ¾; this procedure essentially alleviates uncertainties due to surface effects. The result is not sensitive to the scale factor (3/4) that we employed here; scaling the original axis estimates by 1/2 gives virtually the same density.

Instability, elongation, ordering and electrocrystallization

The effect of the external electric field is reflected in geometrical, structural, and dynamical properties of the droplet, displayed in Fig.1, where we show the variation with the applied field of the aspect ration λ= c/a, the molecular diffusion constant D, the normalized dipole moment (per molecule) of the droplet in the field direction (z), $\bar{\mu} = \mu / \mu_F$ (where μ_F the dipole moment of a formamide molecule), and the order paramer $O_6 = < \sum_{k,j \subset nn} N_{nn,k}^{-1} \exp(i6\theta j) >$ expressing the degree of hexagonal order in the droplet, given by

the above average (taken over all the molecules in the droplet, $1 \leq k \leq N$, and if desired over a certain simulation interval), with the angle θ_j (taken for each of the $N_{nn,k}$ molecules (j), that are nearest neighbors (nn) to molecule k), subtended by the vector from the droplet center of mass (cm) to the cm of the k-th molecule and the vector connecting the droplet cm and the cm of jth neighboring molecule. Included also in Fig.1a are snapshots of the droplet for selected values of the electric field. An assembly of representative configurations of the droplet, and some of the associated physical characteristics, taken for various values of the applied electric field, is given in Fig. 2. Certain distinct features and patterns are evident from inspection of Fig. 1, including field-induced shape elongation, ordering, and electric-field-induced crystallization (or electro-crystallization (EE)) that is found to occur for stronger fields. Additionally we observed pronounced hysteresis when the magnitude of the applied field is decreased.

For fields up to 0.5 V/nm the droplet elongates mildly in the direction of the applied field. However, for larger fields the droplet becomes metastable, undergoing a large shape transition between E_{el} = 0.5 V/nm and 0.625 V/nm that is portrayed by a variation in λ from 1.5 to 12 in this range (see Fig. 1a) which results in a needle shaped droplet (see upper part of Fig. 2). The shape transition is accompanied by an increase in the normalized z-dipole moment from about 0.1 to 0.7 (Fig. 1d). Throughout the elongation transition (with gradual elongation continuing past the shape-transition, for fields in the range of 0.625 V/nm < E_{el} < 1.4375 V/nm the droplet remains liquid (see the diffusion constant D and the order parameter O_6 in Fig.1b and 1c for E < 1.4375 V/nm, respectively); note the gradually diminished molecular diffusivity for fields in the range of 1 V/nm and 1.4375 V/nm.

Shape instability of dielectric droplets at critical electric fields have been the subject of earlier studies (refs R25, R31). Taylor (ref R31, R25) predicted theoretically that a droplet of initial radius R (under field-free conditions) will undergo instability for an external field strength E satisfying (MKS units) $E(4\pi\varepsilon_0 R/\gamma)^{(1/2)}=1.625$. Using, for the droplet studied here, $\gamma = 0.046$ N/m for the computed surface tension and R=4.84 nm for the computed equimolar radius, yields a predicted critical field $E_{e\,l}= 0.48$ V/nm, which is only slightly lower than the field found in our simulation at the onset of instability leading to the shape transition; when the experimental surface tension $\gamma = 0.057$ N/m is used in the above, the predicted critical field strength is 0.53 V/nm.

At a field of 1.4375 V/nm a second critical filed is reached, signaled by a small, but discontinues, change in shape (further elongation to $\lambda \approx 20$), and an increase in $\overline{\mu}$), and, more remarkably, by a precipitous increase in the hexagonal order in the droplet and concomitant discontinuous vanishing of the molecular diffusion in the droplet. These changes are the result of a field-induced electrocristallization (ee) phase transition occurring at E_{ee}. No essential changes occur for higher fields.

When the strength of the electric field is lowered from the of electrocrystallized state the system exhibits a hysteretic behavior. Two transitions are found. The first occurs near 1 V/nm, where solid/liquid (sl) coexistence emerges; see middle and bottom configurations displayed in Fig. 2, where the middle (small z) region of the droplet is characterized by crystalline order, while the regions closer to the droplet ends are liquid-like (note the needle shaped droplet with $\lambda \approx 19$ shown in the middle of Fig.2, exhibiting a non-uniform distribution of the (normalized) dipole moment ($\overline{\mu}$) with the lower values at the droplet's ends reflectig a reduced degree of dipolar alignment at these disordered

regions. As the field is further decreased the crystalline middle region gradually reduces in size. However, while the diffusivity and the degree of hexagonal order are seen to attain liquid-like values near E_{sl} (see Fig.1, although the end regions of the droplet are more disordered then the shrinking middle, with full disorder found only near E=0.7 V/nm)), the elongation (λ) and z-dipole order parameters correspond to an elongated and molecularly aligned (relatively high $\overline{\mu}$) droplet. Generally, we may summarize that the trends observed during the solid/liquid coexistence stage are essentially the reverse of those seen when the liquid droplet approaches the electrocrystallization transition from lower fields.

The second hysteretic feature occurs for the liquid-lile droplet that persists in the elongated and molecularly aligned state (characterized by relatively high values of λ and $\overline{\mu}$) till E=0.375 V/nm), see Fig. 1. This type of hysteresis has been addressed in a number of studies (refs. R12, R23).

We conclude this section with observations that we made from both constant temperature and constant energy simulations pertaining to the state of the droplet after switching-off (suddenly) of the electric field, starting from a highly ordered state, (e.g. E=3 V/nm). In both simulations we found that the time-evolution for the return of the droplet to the original spherical liquid disordered state is exponential with a time constant of ~200 ps. In the constant energy simulation, the temperature of the droplet decreases (since in the recovery process the potential energy increases, i.e. becomes less negative) from its initial 310K to 283K (which is essentially the same as the bulk freezing point of 285K determined by us for the simulated fluid, see discussion above).

We have noted also that the state of the droplet at high field strength can be ordered or disordered depending on the temperature so that there is an interplay between temperature and applied field strength in the phase behavior of the dielectric droplet. Taking the polar fluid to a high field strength state of polarization saturation is analogous to the 'poling' process used to align dipolar domains in ferroelectric materials (ref R37) in which a high dc electric field is applied to a sample at an elevated temperature and after the domains are sufficiently aligned, the temperature is lowered back to room temperature (in the presence of the field) to 'lock in' the highly aligned state. This analogy suggests variations of our study in which the temperature of an ordered polarized droplet at high field strength is lowered dramatically to see to what extent the polarization and order can be 'locked in' and what behavior will be observed under variations of the applied field.

V. COMPARISON TO CONTINUUM THEORY

The energetics and response of a dielectric droplet in a uniform external electric field have been the subject of a number of theoretical studies (refs. R12, R23-R25). The droplet shape is usually taken to be axisymmetric, similar to the experimentally observed shapes, as well as the ones obtained from minimization of formulated free energy models via droplet shape variation, as a function of the applied external electric field (refs R23, R27, R36). There have also been reports on studies based on a force balance approach, where the balance between the electrical and capillary stresses across the droplet surface are considered (R12,23-25,31,33); in some of these approaches non-linear polarization effects have been considered (R33). The droplet surface is often modeled as a prolate (elongated) spheroid, PS, which captures the basic overall shape of a droplet undergoing

elongation in an electric field. More complex droplet shapes, such as conical droplet ends that can form under certain circumstances, were considered in more detailed studies (see R12 for review).

The wealth of detailed information generated in our MD simulations allows us to explore and asses the appropriateness of continuum based models for the description of the behavior of nano-scale droplets. Such evaluations led us to introduce a new free-energy model in which the shape of the dielectric droplet is represented as a prolate spheroid, but unlike previous models the dielectric constant of the droplet is taken to depend on the strength of the applied electric field. This leads to a new term in the expression for the free-energy. We will show that these modifications to the standard PS free-energy model bring the results of the model into excellent agreement with our atomistic MD simulations. Since the novel aspects of our model are associated with non-linear dielectric properties we will refer to out model as the NLPS (non-linear prolate spheroid) model.

At this point it is pertinent to define certain relevant quantities that are needed in the subsequent discussion. We note that MKS units will be used by us here; this involves scaling in some of the equations by a factor of $4\pi\varepsilon_0$ in comparison to the usage of Gaussian units.

A. Dielectric Droplets in Strong Electric Fields

When a fluid droplet made up of polar molecules is subject to an external electric field, the resulting field inside the droplet causes both an induced polarization of molecular charge and a polarization due to dipole orientation. For small field strengths

the polarization (dipole moment per unit volume) varies linearly with the internal field strength, $\mathcal{P}=P/V = \varepsilon_0(\varepsilon-1)E$, where ε is the relative permittivity, or dielectric constant (R27,36). For larger applied fields, the competition between thermal and polarization effects leads to a non-linear relation between the polarization and the field

$$\mathcal{P}= P/V =\varepsilon_0(\varepsilon(E)-1)E, \tag{5.1}$$

Commonly, the field dependent permittivity $\varepsilon(E)$ continues to be refereed to as the dielectric "constant". The study of non-linear dielectric saturation effects and in particular the response of polar fluids to high field strengths has a long history and it remains an active research area up to date (R32-35,43).

In modeling the droplet surface as that of a prolate spheroid (PS), the assumption is normally made that the volume of the droplet remains constant as the droplet undergoes elongation, namely $V=4\pi/3a^2c=4\pi/3R^3$ where c and a are the semi-major and -minor axes of the ellipsoid and R is the radius of the initial spherical droplet when under field-free conditions. The symmetry axis of the ellipsoid is taken as the z-axis and unless otherwise stated the field and dipole components discussed below are understood to be the z-component. Denoting the droplet's aspect ratio as $\lambda=c/a$, the eccentricity, e, is given by $e^2=1-1/\lambda$. We assume the droplet is surrounded by a vacuum (dielectric constant of unity).

As aforementioned, an important point of departure of this work from previous investigations is that the dielectric constant of the fluid droplet is taken as a material dependent quantity that is a function $\varepsilon(E)$ of the internal electric field strength E inside

the fluid. The field strength E (understood to be along z) inside a prolate spheroid subject to a uniform parallel external field E_0 is the sum of E_0 and the opposing field created by the induced polarization charges

$$E = E_0 - (P/V)n(\lambda)/\varepsilon_0 , \tag{5.2}$$

where P is the ellipsoids total dipole moment along z and $n(\lambda)$ is the z-component of the depolarizing factor (ref R27,36). $n(\lambda)$ is a function of the eccentricity, $e(\lambda)$, and therefore the aspect ratio λ through the implicit relation $n(\lambda)=(1-e^2)(\ln[(1+e)/(1-e)]-2e))/(2e^3)$. The two relations (Eqs. 5.1and 5.2) give

$$E_0 = [1+(\varepsilon(E)-1)n(\lambda)]E , \tag{5.3a}$$

and

$$P = \varepsilon_0 V(\varepsilon(E)-1)/\{1+(\varepsilon(E)-1)n(\lambda)\}E_0 . \tag{5.3b}$$

We note that Eq. 5.3b, along with the definitions in the preceding paragraph, enables one to compute, using data from the MD simulation, the field-dependent dielectric constant $\varepsilon(E)$ for a droplet having an interior field E with an external field E_0. For a given imposed external field strength, E_0, the simulations allow us to obtain time averaged values for the droplet's dipole moment, P, the semi-major and –minor axes (c and a), aspect ratio λ , associated droplet volume V, eccentricity and depolarizing factor

$n(\lambda)$. These values are then used with Eq. 5.3b to obtain the dielectric constant $\varepsilon(E)$ as a function of both E and E_0 since E may be computed using Eq 5.3a.

The dielectric constant computed as a function of the *external* field strength E_0 from the MD simulations using Eq 5.3b is shown in Fig. 3 (symbols). We observe a general monotonic decrease of the dielectric constant for increasing field strengths, which is consistent with experimental results for various liquids subjected to similar field strengths as those used in our simulations (ref R34-35). The different symbols in Fig. 3 give information on the manner in which dielectric constants were computed. The filled symbols in Fig 3 correspond to MD equilibrations in which the external field E_0 (constant for each run) was raised from the field of a preceding equilibration; namely, the configuration at the end of a long equilibration performed at a lower external field serves as the a starting point for a subsequent simulations performed for an incremented (increased) value of the applied filed. The empty symbols correspond to the reverse process where the end configuration from a simulation performed for a given value of the applied field, serves as the starting one for a subsequent simulation at a lower value of the field; comparison between the curves corresponding to the filled and empty symbols allows us to explore hysteretic effects. The circles in Fig. 3 are associated with the use of the prolate spheroids total dipole moment P and volume V in Eq 5.3b; the squares (and triangles) use a PS volume inside the droplet whose semi-major and –minor axes are ¾ (and ½) the length of the full PS. While the results using these different averaging volumes agree rather well, those that use an averaging volume inside the droplet show less variation at the lower fields.

As will be discussed below the internal electric field strength is a function $E(E_0, \lambda)$ of both the external field (E_0) and the droplet's aspect ratio (λ), and points in Fig 3 below $E_0 \sim 0.5$ V/nm correspond to a much smaller range of internal fields ($E < 0.05$ V/nm); consequently, equilibration at such low values of E_0 are characterized by poorer statistics as regards the calculation of the dielectric constant. One observes in Fig. 3 a pronounced hysteretic behavior of the dielectric constants that correlate with the corresponding hysteresis that characterizes the evolution of in other physical properties of the droplet as a function of the applied field (see Fig 1), as the droplet undergoes transitions between different states. The heavy curve in Fig. 3 (between the two vertical dashed lines) depicts to a fit of the MD dielectric constants to a theoretical curve relating $\varepsilon(E)$ to the internal field (E), plotted versus the external field E_0;

In order to explore the predictions of the NLPS model, with its non-linear dielectric saturation effects, we fit the observed dielectric constants $\varepsilon(E)$ (Fig. 4) with an approximation that has been found useful (ref R34,35) in the description of experimentally observed saturation effects, i.e.,

$$\varepsilon(E) = n^2 + \alpha/E \, L(\beta E) , \qquad (5.4)$$

where $\alpha = a/s_1$, $a = \rho(n^2+2)\mu_0/(3\varepsilon_0)$, $\beta = s_2 b$, $b = (n^2+2)\mu_0/2k_BT)$, n is the optical refractive index (n=1 for the non-polarizable formamide model used here), $\mu_0 \sim 0.08087$ q-nm (3.88 Debye) is the molecular dipole moment, $\rho \sim 14.7$ molecules/nm^3 is the liquid density, k_B is Boltzmann's constant, T=310K and $L(x)=\coth(x)-1/x$ is the Langevin function; we use the scaling parameters s_1 and s_2 (of order unity) as fitting parameters.

While other similar functional forms (R35) have been suggested, Eq 5.4 has the merit of retaining the dependence of the dielectric constant on a host of material properties and the values of s_1 and s_2 can serve as comparative measures of the dielectric response to that of other materials. The values $s_1=s_2=1$ gives the Booth-Onsager formula (R34) for simple liquids with relatively small molecular dipole moments while $s_1= \sqrt{73}/7 \sim 1.22$, $s_2= \sqrt{73}/3 \sim 2.85$ give the Booth-Kirkwood formula (R34) in which nearest neighbor correlations due to the hydrogen bonding (in water) are taken into account in performing ensemble averaging. Expressing the electric field in units ofV/nm as the units of the, and using the appropriate parameters for our system, we find for the coefficients a and b (defining α and β in Eq. 5.4) the values a=21.5 V/nm and b=4.53 $(V/nm)^{-1}$.

Because of the large variation in the results obtained in our simulations for internal fields less than 0.05 V/nm, we restrict ourselves to results corresponding to larger fields (i.e. E>0.05 V/nm) in the fitting analysis. The solid curve in Fig. 4 uses dielectric constants computed inside an internal "¾" size PS, as discussed above, and Eq (5.4) with $s_1=0.947$ and $s_2=1.117$; a similar result is obtained for the "½ " size internal averaging volume. It is of interest to note to that Eq 5.4 provides such a good description of the simulation data with the values of the adjustable parameters s_1 and s_2 close to unity, as this is the limiting case of using the appropriate density, dipole moment and temperature for the system being studied with no adjustable parameters.

There are a number of interesting features pertaining to the results displayed in Figs. 3 and 4 that merit further notice. For the low-field range, where any elongation of the droplet is essentially insignificant (see Fig. 1a before the shape transition the internal electric field is much smaller than the corresponding external field.), However, when the

external field E_0 attains a value that just exceeds the critical field (~ 0.5 V/nm), leading to shape instability of the droplet, the internal field E, along with many properties of the droplet vary largely in a rather marked manner (Fig 1). Note also that in the transition region from liquid to crystalline droplet of Fig 4 (E ~ 1.2 V/nm) the curves corresponding to the liquid and ordered states run (essentially) parallel to each other, and thus two different values of for the dielectric constant (one for the liquid and one for the ordered droplet) may be obtained in this region for the same internal field E.

One of the most intriguing observations that we made concerns the finding that the droplet transforms from a liquid to a solid phase when the dielectric constant $\varepsilon(E)$ (decreasing in magnitude with increasing field E) just reaches the value $\varepsilon(E_{liq\text{-}sol}) \sim 18$. In studies of the stability of dielectric drops in electric fields (with no saturation effects, see R12 for a review), it has been found that when the dielectric constant ε exceeds a value of about 18, there are two distinct solutions for the droplet shape having conical ends, while for $\varepsilon < 18$ there is only a single solution having rounded droplet ends. In the context of our study, we may conclude that: when $\varepsilon(E)$ is above ~18, there are conditions involving interfacial stress balances that restrict the possible shape of the droplet near its ends. However, when the value of $\varepsilon(E)$ drops below ~18, these restrictions are relaxed, and concomitantly crystalline order emerges. This suggests that the transition from a liquid droplet to one with crystalline symmetry, and the associated different boundary conditions and geometry, is inhibited by the interfacial stresses occurring above $\varepsilon(E)$ ~18 that may drive the droplet to geometries inconsistent with a nascent crystalline form.

It is important to note that the foregoing relations between E_0, E and $\varepsilon(E)$ may be used to write a defining relation of the electric field strength inside the droplet (E) as a

unique function $E(E_0,\lambda)$ of the applied field E_0 and aspect ratio λ. Using the expression for $\varepsilon(E)$ given in Eq 5.4 in Eq 5.3a, one can write (in dimensionless form) a determining relation for the field strength E in terms of E_0 and λ,

$$x_0 = x + c(\lambda)L(x)\,, \tag{5.5}$$

where $x_0=s_2bE_0$, $x=s_2bE$, and $c(\lambda)= abn(\lambda)s_2/s_1$. For given E_0 and λ (or x_0 and λ) there is a unique solution, x, to Eq 5.5, which may be easily found using a simple iterative method. Consequently, for analytical purposes, the internal field strength inside the droplet may be viewed as a given continuous function $E(E_0,\lambda)$ of the external field and the droplet aspect ratio.

B. Free energy and it's minimization

When the dielectric constant of the droplet fluid is taken to be independent of the internal electric field, the total free energy in the prolate spheroid (PS) model, $F_{PS}= F_{polz} + F_{surf}$, consists of an electrical polarization term $F_{polz}=-1/2\ PE_0$ and a surface energy $F_{surf}=\gamma A$, where A is the surface area of the PS (ref 23 more), E_0 and E are the external and internal electric field along the z-axis, and P is the total dipole moment of the droplet along the z axis (see Eqs 5.1-5.3). When the dielectric constant is allowed to vary with the internal field strength an additional term is necessary in order to obtain a free energy consistent with the thermodynamic relation (R27) (at constant temperature)

$$dF = -PdE_0\,. \tag{5.6}$$

The integrated form of this relation for the NLPS model is

$$F_{NLPS} = -1/2\ PE_0 + \gamma A(\lambda) + V\varepsilon_0/2 \int_0^{E(E_0,\lambda)} E^2\, \varepsilon'(E) dE\,, \qquad (5.7)$$

where $\varepsilon'(E)$ is the derivative of ε with respect to the internal electric field and the reference point of the free energy is the state with vanishing external field. The third term, which we denote by F_{sat}, is associated with saturation effects and is absent when the dielectric constant is independent of field strength. The form of the free energy may be rewritten in various ways, having different interpretations. For example, one could replace $E^2\, \varepsilon'(E)$ in the integrand of F_{sat} by $E(\varepsilon_d(E)-\varepsilon(E))$ where the derivative of the displacement field $\varepsilon_d=1/\varepsilon_0 dD/dE$ is the differential dielectric constant which has been found useful in the study of dielectric saturation phenomena (R35).

As discussed earlier, the electric field, E, inside the droplet may be considered as a well defined function of E_0 and λ so that the dipole moment of the droplet P given in Eq 5.3b may also be viewed as a function of E_0 and λ. The free energy in Eq 5.7 is therefore a function of the applied external field, E_0, which can be viewed as an external control variable, and the droplet's aspect ratio, λ, which characterizes the droplets response to the applied field as well as it's state of thermodynamic equilibrium. In the differential $dF=\partial F_{NLPS}/\partial E_0 dE_0 + \partial F_{NLPS}/\partial\lambda\ d\lambda$, one finds from direct differentiation of Eq 5.7 that $\partial F_{NLPS}/\partial E_0 = -P$, while the second term is set to zero, $\partial F_{NLPS}/\partial\lambda = 0$, as this is the condition that the droplet responds to the applied field by a change in aspect ratio, so as to minimize the free energy (also $\partial^2 F_{NLPS}/\partial\lambda^2 > 0$). In performing these differentiations, one uses the explicit functional dependence of the free energy on E_0 and λ, e.g. Eq 5.3b.

Also, it is interesting to note that the derivative of the integral saturation term, $(V\varepsilon_0/2)\,E^2\,\varepsilon'(E)\;\partial E(E_0,\lambda)/\partial E_0$ (or $\partial E(E_0,\lambda)/\partial\lambda$) cancels exactly identical terms arising from differentiaion of the polarization term with respect to E_0 or λ . As a result of these cancellations, $\partial F_{NLPS}/\partial E_0$ and $\partial F_{NLPS}/\partial\lambda$ give the same functional form as when there is no saturation term, e.g. $\partial F_{NLPS}/\partial E_0 = -P$. Also the condition $\partial F_{NLPS}/\partial\lambda = 0$ gives a relation between the derivatives of the depolarizing factor and area, $n'(\lambda)P^2/(2\varepsilon_0 V)+\gamma A'(\lambda)= 0$ that is true both in the original PS model as well as the NLPS model where saturation effects are included. It is interesting to note here that the latter equation leads to a simple relation, between the pressure inside the undistorted droplet, the droplet polarization, and purely geometrical factors

$$\mathcal{P}/\varepsilon_0 = (3\Pi_0/\varepsilon_0)^{1/2}\, g(\lambda)\,, \tag{5.8}$$

where $\Pi_0=2\gamma/R$ is the pressure inside the droplet of radius R at zero field, $g(\lambda) = [-A'(\lambda)/A_0/n'(\lambda)]^{1/2} = [-d\tilde{A}/dn]^{1/2}$, $A_0=4\pi R^2$, and $\tilde{A}=A(\lambda)/A_0$.

Using the expression for $\varepsilon(E)$ given in Eq 5.4, one can evaluate the saturation integral term F_{sat} in the free energy expression (Eq 5.7). The result may be written as

$$F_{sat} = -1/2\ PES(x)\,, \tag{5.9a}$$

$$S(x) = 2\ln\,[\sinh(x)/x)/(xL(x)] - 1\,, \tag{5.9b}$$

where ln [ ] is the natural logarithm and $x=s_2bE$ (as in Eq 5.5). The free energy $F_{NLPS}=F_{polz}+F_{surf}+F_{sat}$ can now be written as

$$F_{NLPS}(E_0, \lambda) = -1/2\ PE_0 + \gamma A(\lambda) - 1/2\ PES(x)\ , \qquad (5.10)$$

with the explicit reminder that all of the variables involved are functions of E_0 and λ. P is given in Eq 5.3b in terms of E, $\varepsilon(E)$ and $n(\lambda)$. $\varepsilon(E)$ is given in Eq 5.4 and $E(E_0, \lambda)$ is uniquely determined from Eq 5.5. The 'saturation' function S(x) has the limits S(0)=0 and $S(x)\rightarrow 1$ for large x so that for large external, and associated internal fields, the new term in the free energy, F_{sat} , approaches −1/2 PE. As has been discussed earlier, the droplet may change phase in sufficiently high fields and the above analysis will be modified.

In studies of fluid droplets interacting with external fields such as gravitational or electrical fields, and possibly in the presence of surfaces where interfacial energies play a role, it is common to define dimensionless numbers, called Bond numbers, that characterize the ratio (and relative importance) of the various body forces to surface tension forces at the liquid interfaces. Gravitational and electrical Bond numbers are common. In studies of droplets in electric fields, an electric Bond number $B_E=\varepsilon_0 E_0^2 R/\gamma$ is frequently used, where γ is the surface tension, expressing the ratio between electrical polarization forces, tending to elongate the droplet, to capillary forces tending to contract the droplet; depending on the particular variants of the above definition are sometime used. We will employ here the definition of B_E given above, and we normalize the energies to a dimensionless form by dividing them by the surface energy of the undeformed droplet: $F_{PS} \equiv (F_{PS}/(4\pi R^2\gamma)$ and similarly for it's components. For our system $4\pi R^2\gamma \sim 0.0119$ eV/molecule. We have (see refs. R23, R27)

$$F_{NLPS}=F_{polz}+F_{surf}+F_{sat}\ , \tag{5.11a}$$

$$F_{polz}=-(B_E/6)(\varepsilon-1)/\{1+(\varepsilon-1)n\}\ , \tag{5.11b}$$

$$F_{surf}=(1/2)(1-e^2)^{(1/3)}[1+(\sin^{-1}e)/(e(1-e^2)^{(1/2)})]\ , \tag{5.11c}$$

$$F_{sat}=F_{polz}\,(E/E_0)S(x)\ . \tag{5.11d}$$

For a given value of the external field E_0, the energy F_{NLPS} is a function of the droplet shape through the aspect ratio λ, appearing in the eccentricity $e(\lambda)$ and internal electric field $E(E_0,\lambda)$, and it may exhibit one or more local minima or maxima with respect to variations of λ. The values of the aspect ratio λ associated with minima of F_{NLPS} define the stable (or metastable) droplet shapes (ref R23). We will perform the variation of the aspect ratio numerically to find the predicted stable configurations of the droplet for a wide range of external fields and compare a number of predictions from the above NLPS model, based on continuum macroscopic theory, with results of the MD simulations. Specifically, for a given field E_0 we assume an initial value of the aspect ratio λ=1 and vary λ in small increments ($\Delta\lambda$=0.01), evaluating the free energy and recording the extremal points for each value of E_0. Key ingredients in this model are the new free energy contribution F_{sat}, the function $\varepsilon(E)$ determined as described above using MD results, and the internal field strength $E(E_0, \lambda)$ which is obtained using Eq 5.5 in the course of the incremental λ search for each external field E_0.

The aspect ratios of the droplet deduced directly from the MD simulation data by means of axial and radial binning of the molecular number density (described earlier, see sec. IV) are shown in Fig. 5 (symbols) as a function of the electric bond number B_E. The aspect ratios that were found to minimize (through the numerical search procedure outlined above) the NLPS free energy for each value of E_0 are given as the solid curves. The regions associated with field strengths below $E_0 \sim 0.5$ V/nm and above ~ 0.625 V/nm (the black curves) correspond to the NLPS free energy F_{NLPS} having exactly one minimum with respect to the aspect ratio. Within the S-shaped region ($E_0 \sim 0.5$ - 0.625 V/nm), there are two minima (black and gray segments) and one maximum (dashed segment). We call attention to the very good agreement that is found between the MD results and the predictions of the NLPS model developed here. In particular, note the MD point (open symbol) that was obtained by lowering the applied field from a stable configuration into the metastable region (gray curve).

It is of particular interest to assess the contribution of the saturation term. The predicted aspect ratios obtained from the NLPS (and PS) model are shown in Fig. 5 (upper dashed line) up to the point of droplet crystallization for a model where one takes the dielectric constant of the droplet to be independent of field strength (the normal PS model) and equal to the zero field value $\varepsilon(E=0) \sim 39.2$ (see footnote R46). If the dielectric constant $\varepsilon(E)$ is allowed to vary, but the dielectric saturation term F_{sat} is not included in the free energy minimization, the predicted aspect ratios vary as depicted by the lower dashed curve in Fig 5. From these results we conclude that the saturation term is essential for a correct description of the field-induced droplet shape.

One can compute the free energy via several routes. Besides the minimization of the NLPS model free energy described above one may also use the MD results and the basic relation in Eq 5.6 to evaluate directly

$$F_{MD} = -\int_0^{E_0} P_{MD}(E_0)dE_0 \,, \tag{5.12}$$

where $P_{MD}(E_0)$ is a piecewise polynomial fit to the calculated dipole moments of the droplet (proportional to the data presented in Fig. 1d). We present in Fig. 6 the free energies obtained from both the MD results, F_{MD}, and the NLPS model, F_{NLPS}. The energies are normalized through division by the surface energy at zero field $F_{surf0} \equiv 4\pi R^2\gamma$ (~0.0119 eV/molecule), resulting in the NLPS free energy F_{NLPS} being equal to unity at E_0=0. The normalized free energy, F_{MD}, from the MD data is shifted upward by 1.0 for comparison with F_{NLPS}.

The free energy F_{MD}, Eq 5.12, obtained directly from the MD data (shown as a dashed line in Fig. 6) is in remarkable agreement with the numerical minimization of the free energy F_{NLPS} (Eqs. 5.7, 5.10-5.11) based on the non-linear prolate spheroid model. As was done with the aspect ratios (Fig 5), we show the predicted free energies (light dashed lines) obtained when a non-varying dielectric constant is used, $\varepsilon=\varepsilon(E=0)$, or when a non-constant $\varepsilon(E)$ is employed but asaturation term is not included in the free energy expression. This reaffirms our conclusion concerning the importance of including the term describing saturation effects in the free energy.

The individual contributions to the free energy, arising from the polarization, surface and saturation terms, are displayed in Fig. 7. We show the predictions of the NLPS model, developed for a fluid droplet, up to the point of droplet crystallization. However for the more general MD free energy (Eq 5.12) we extend the integration into

the ordered droplet region. We can also calculate the polarization, surface and saturation terms based solely on the configuration of the droplet as given by the MD data (this does not involve any minimization). These contributions are depicted by the dashed curves in Fig. 7, and they are fund to overlap those predicted by our model (shown by the solid curves).

It has been noted (R27) that an increase in the permittivity of a medium should result in a lowering of the free energy. In the present case, we find a lowering of the dielectric constant relative to its zero field value and one should expect a resulting *increase* in the free energy. This is not immediately apparent from Eqs 5.7, 5.10 and 5.11 where the saturation term is strictly negative. However, we note from Fig. 6 that the free energy is in fact always larger than the values it would have if one employed a constant dielectric constant. The effects of a varying dielectric constant also influence the polarization term F_P of the free energy and it is the minimization of the total free energy with respect to the aspect ratio, involving the interplay of all of the contributions to it, that determines the droplets state and free energy.

A most interesting relationship is found the variations in the surface energy and the contributions to the droplets potential energy arising from the Van der Waals (VdW) component of the internal energy. The normalized surface energy is $\gamma\, \mathcal{A}(\lambda) / (\gamma\, \mathcal{A}(\lambda=1)$ (where $\mathcal{A}(\lambda)$ is the area of the prolate spheroidal droplet) and it is a function of the shape of the droplet only (Eq. 5.11c). This is shown as the upper dashed curve in Fig. 7 and was computed using polynomial fits to the observed MD aspect ratios λ. The VdW contributions to the internal energy, averaged for each MD equilibration (also normalized by dividing by $4\pi R^2\gamma$ ~0.0119 eV/molecule and shifted to 1.0 in order to coincide with

$F_{surf}(E_0=0)$) is shown in the upper part of Fig 7 (triangles). Up to the droplet crystallization point we find close correspondence between the variations (from zero field) of the Van der Waals internal energy contributions and the variations of the surface energy (even in the metastable region). Crystalline ordering of the droplet is accompanied by a drop of the VdW energy to its low field value (i.e. $E_0 \leq 0.5$ V/nm). Thus, in the liquid regime the variations in surface energy of the droplet are closely related to variations in the VdW potential energy. Since the surface energy relates to the reduced number of nearest neighbors for molecules located at the surface region, it is reasonable to expect that variations in the short-range VdW interactions will indeed correlate with variations in the surface energy.

C. Entropy

To gain a better understanding of the driving forces behind the field-induced structural changes of the droplet, we compute changes in free energy and entropy that are associated with the droplets response to the applied electric field. Taking the zero electric field point as a reference, the changes in Helmholtz free energy are given by $\Delta F=\Delta U-T\Delta S$, in which ΔU and ΔS are the changes in internal potential energy and entropy, respectively as the electric field E_0 is raised. The calculation of the free energy $\Delta F=F_{MD}$, through numerical integration of the polarization energy (Eq 5.12), was described in the preceding section and is shown in Fig 8. Along with the free energy F_{MD}, we display again in Fig 8 (dashed line) the free energy of the non linear prolate spheroid model, ΔF_{NLPS} (given relative to it's value for zero field), as obtained from the minimization of the prolate spheroid free energy, to illustrate the remarkable agreement

between the MD and analytical model results (note that the energies are again scaled by the zero field surface energy).

The potential energy ΔU_{MD} shown in Fig 8 was obtained as a piecewise polynomial fit to the time-averaged potential energies obtained from the MD equilibration for each applied field E_0. The marked drop in potential energy that occurs when the droplet orders corresponds to a latent heat (enthalpy of fusion) $\Delta H \sim 0.045$ eV/molecule or ~4.3 kJ/mole (the experimental enthalpy of fusion for bulk formamide at 276K is ~ 8 kJ/mole, ref. R42).

The entropic contribution to the free energy, $-T\Delta S = \Delta F - \Delta U$, is also shown in Fig 8. We find in the low field region (E_0 less than 0.5 V/nm) prior to elongation of the liquid droplet that $-T\Delta S$ and ΔU are both negative, with essentially the same magnitude, and the two become more negative as E_0 increases and approaches the point of instability. The entropy therefore *increases* with field strength for small droplet elongations where the field may only influence the molecular coordinates only slightly. Subsequent to the sharp transition of the droplet to a more highly elongated state, the molecular dipoles become more highly aligned and the entropic term $-T\Delta S$ changes sign and takes positive values, a opposite to the internal energy ΔU, and it makes a large contribution to the free energy, corresponding to a *lowering* of the entropy of the droplet as the field is increased further. The entropy decreases roughly linearly with the external field strength E_0 and the entropic component, $-T\Delta S$, of the free energy change remains about 1/3 the magnitude of the potential energy component ΔU. The entropy of fusion, given by $\Delta H/(310K)$, is ~ 14 J/mole^{O}K (the experimental value for bulk formamide is ~30 J/mole^{O}K, ref. R42). We

note that a depression in the enthalpy and the entropy of melting for nano-scale clusters is a current topic of both experimental and theoretical interest (Refs. R44 and R45).

ACKNOWLEDGEMENTS

This research has been supported by a grant from the Air Force Office of Scientific Research.

REFERENCES

R1) M. P. Allen and D. J. Tildesley, *Computer Simulation of Liquids* (Clarendon, Oxford, 1987)

R2) M. Svanberg, Mol. Phys. **92**, 1085 (1997).

R3) E. D. Stevens, Acta Cryst. **B34,** 544 (1978).

R4) W. D. Cornell, et al., J. Am. Chem. Soc. **117**, 5179 (1995).

R5) www.amber.ucsf.edu/amber/ff94/parm.dat

R6) E. Sigfridsson and U. Ryde, J. Comp. Chem. **19**, 377 (1998).

R7) L. Perena, et al., J. Chem. Phys. **102**, 450 (1995).

R8) L. F. Greengard, *The Rapid Evaluation of Potential Fields in Particle Systems* (The MIT Press, 1988).

R9) **No Need Now** The physics is not expected to be significantly different than for T=300K. Nevertheless, we work at a slightly higher temperature 310K to account for the 9°K higher melting point of the simulated formamide so that our results correspond more closely to 300K experimental results.

R10) M. Gamero-Castano and V. Hruby, J. of Propulsion and Power **17,** 977 (2001).

R11) M. Gamero-Castano and J. Fernandez de la Mora, J. Chem. Phys. **113**, 815 (2000).

R12) H. A. Stone, J. R. Lister, and M. P. Brenner, Proc. R. Soc. London A **455,** 329 (1999) (contains a good review of prior work).

R14) M. Moseler and U. Landman, Science **289**, 1165 (2000).

R15) T. K. Xia, J. Ouyang, M. W. Ribarsky and U. Landman, Phys. Rev. Lett. **289**, 69 (1992).

R18) J. Fernandez de la Mora and I. G. Loscertales, J. Fluid Mech. **260**, 155 (1994).

R19) I. G. Loscertales, and J. Fernandez de la Mora, J. Chem. Phys. **103**, 5041 (1995).

R20) surf tension calc. method ref

R21) D. R. Lide (ed.), *CRC Handbook of Chemistry and Physics 85th Ed.* (CRC Press, New York, 2004)

R22) dielectric constant calc. of a sph. droplet; theory, etc. more

R23) J. D. Sherwood, J. Fluid Mech. **188**, 133 (1988); We note that the electrical polarization energy in this ref has several typos. Also note that the definition of electric bond number here is a factor of two larger than the definition in ref R12.

R24) J. D. Sherwood, J. Phys. A: Math. Gen. **24**, 4047 (1991).

R25) O. A. Basaran and L. E. Scriven, Phys. Fluids A **1**, 799 (1989).

R26) J. G. Powles, R. F. Fowler and W. A. B. Evans, Chem. Phys. Lett. **107**, 280 (1984).

R27) L. D. Landau and E. M. Lifshitz, *Electrodynamics of Continuous Media* (Pergamon, New York, 1960).

R28) J. W. Essex and W. L. Jorgensen, J. Phys. Chem. **99**, 17956 (1995).

R29) U. Landman, C. L. Cleveland, and C. S. Brown, Phys. Rev. Lett. **45**, 2032 (1980).

R31) G. I. Taylor, Proc. R. Soc. Lond. A **280**, 383 (1964).

R32) J. G. Powles, M. L. Williams and W. A. B. Evans, J. Phys. C: Solid State Phys. **21**, 1639 (1988).

R33) F. K. Wohlhuter and O. A. Basaran, J. Magnetism and Magnetic Materials **122**, 259 (1993).

R34) F. Booth, J. Chem. Phys. **19**, 391,1327,1615 (1951),

R35) J. Liszi, L. Meszaros and I. Ruff, J. Chem. Phys. **74**, 6896 (1981).

R36) J. A. Stratton, *Electromagnetic Theory* (McGraw-Hill, New York, 1941).

R37) M. E. Lines and A. M. Glass, *Principles and Applications of Ferroelectrics and related Materials* (Clarendon Press, Oxford, 1977).

R38) H. Li, T. C. Halsey and A. Lobkovsky, Europhys. Lett. **27**, 575 (1994).

R39) J. Ladell and B. Post, Acta Cryst. **B7,** 559 (1954).

R40) K. P. Sagarik and R. Ahlrichs, J. Chem. Phys. **86**, 5117 (1987).

R41) H. J. C. Berendsen, J. P. M. Postma, W. F. van Gunsteren, A. DiNola, and J. R. Haak, J. Chem. Phys. **81**, 3684 (1984).

R42) NIST Chemistry WebBook, http://webbook.nist.gov/chemistry

R43) H. Frohlich, *Theory of Dielectrics*, (Oxford University Press, New York, 1949).

R44) M. Schmidt, R. Kusche, B.v.Issendorff and H. Haberland, Nature **393**, 238 (1998).

R45) Q. Jiang, C.C. Yang and J.C. Li, Materials Letters **56**, 1019 (2002).

R46) The zero field dielectric constant that we find for liquid formamide (~39.2) is lower than the experimental value of ~111. It has been noted (ref 28) that fixed charge models tend to underestimate the dielectric constant. For a study such as this, it is important to use the material constants determined specifically for the model fluid being used in developing ideas and theoretical models in a consistent manner

FURTHER REFERENCES

L1) G. I. Taylor, "Disintegration of Water Drops in an Electric Field", Proc. R. Soc . **A280**, 383 (1964); "Electrically Driven Jets", *ibid.*, **A313**, 453 (1969). In this context we note the original observations by J. Zeleny, "On the Conditions of Instability of Electrified Drops, with Applications to the Electrical Discharge from Liquid Points", Proc. Camb. Phil. Soc., **18**, 71 (1915), and "Instability of Electrified Liquid Surfaces", Phys. Rev. **10**, 1 (1917).

L2) A. G. Bailey, *"Electrostatic Spraying of Liquids"*, (Wiley, New York, 1988).

L3) K. Tang and A. Gomez, "Generation by Electrospray of Monodisperse Water Droplets for Targeted Drug Delivery by Inhalation", J. Aerosol. Sci., **25**, 1237 (1994).

L4) See articles in J. Aerosol. Sci., **25**, No. 6 (1994), Special Issue on "Electrosprays: Theory and Applications"; (b) M. Gamero-Catano and V. Hruby, "Electrospray as a Source of Nanoparticles for Efficient Colloid Thrusters", presented at the 36th AIAA/ASME/SAE/ASEE Joint Propulsion Conference & Exhibit, Huntsville, AL, 2000; (c) D. Michelson *"Electrostatic Atomization"*, (Adam Hilger, Bristol, 1990); (d) See the review in J. Eggers, "Nonlinear Dynamics and Breakup of Free-Surface Flows", Rev. Mod. Phys., **69**, 865 (1997); in particular pp. 919-922, and literature citations therein. This excellent review contains original material as well as a comprehensive discussion and list of references to earlier work on dynamics and breakup processes in liquid jets and other free-surface flow problems.

FIGURE CAPTIONS

FIGURE 1 Averages of droplet properties illustrating a rich variety of both hysteretic behavior and varied types of accompanying correlations in the droplets properties as the applied E-field is raised and lowered. Symbols correspond to points reached either by an increase (filled symbols) or lowering (open symbols) of the E-field. Note that when the droplet undergoes elongation at E~0.5 V/nm, the aspect ratio (a) increases from 1.5 to 12 and the normalized z-electric dipole moment (d) also shows a pronounced increase from ~0.1 to 0.7. However the droplet remains liquid and there are no changes seen in the diffusion constant (b) and O_6 order parameter (c). The liquid droplet elongates gradually until a field of E~1.5 V/nm is reached at which point it crystallizes. The changes in the averages now are opposite to those seen when the droplet initially elongated. The aspect ratio (a) and z-dipole moment (d) change little while the diffusion constant (b) essentially goes to zero and the O_6 order parameter (c) increases dramatically reflecting the liquid to solid transition. Little change is seen for higher E-fields. As the field strength is lowered from the point of crystallization, the droplet does not immediately re-melt but exhibits a hysteretic solid/liquid coexistence to a lower electric field strength of 1 V/nm, below which it returns to the same liquid state conditions as before. The trends seen in the averages during this stage of solid/liquid coexistence are essentially the reverse of those seen when the liquid droplet approached the critical field for freezing: there are very large variations in the diffusion (b) and O_6 order parameter (c), and minor changes in the aspect ratio and z-dipole moment. The averages change gradually until the lowering E-field reaches 0.5 V/nm where it again displays hysteresis in that it does not return to it's

original stats but remains slightly elongated with aspect ratio ~ 8, see (a), and normalized z-dipole moment (d) of ~ 0.4. Below E=0.5 V/nm the droplet returns to its initially unelongated state.

FIGURE 2 Images illustrating the progression of stable states of the formamide droplet as the externally applied electric strength, E, is initially raised (top) and later reduced (bottom). At zero field, the droplet is undistorted with aspect ratio λ=1 which increases to λ=1.5 at E=1.5 V/nm. As the field E is raised above the critical field to 0.625 V/nm, the droplet elongates abruptly to an aspect ratio of λ=12. When the electric field strength exceeds E~1.5 V/nm, the droplet crystallizes, changing little as the field is further increased. As the E-field is lowered, the droplet displays hysteretic behavior (bottom) and exhibits a solid/liquid coexistence until a lower field of 1.0 V/nm is reached at which point the system returns completely to the liquid state. Shown at the bottom are side views showing liquid/solid coexistence, lattice planes as they appear under 30 degree axial rotations of droplet and an end view down the long axis of the entire droplet. Overlaid on the droplet is a curve showing the variation of the average z-component of the electric dipole moment per molecule normalized by the dipole moment of a formamide molecule. The strong correlation seen between the z-dipole moment and degree of droplet order is also reflected in other structural order parameters (e.g. see Fig. 1).

FIGURE 3 Variation of the dielectric constant with the externally applied field strength E_0. One notes the transition to an ordered droplet when E_0~1.4 V/nm (and ε~18) and a pronounced hysteresis as the field is decreased after the droplet has ordered. The thick dark curve derives from a fit of $\varepsilon(E)$ to the Booth-Onsager equation and its use in

the NLPS free energy minimization. Note the predicted metastable region (curved light gray line) and unstable region (curved light dashed lines) for E_0 field values in the range ~0.5-0.6 V/nm.

FIGURE 4 Variation of the dielectric constant with the local field E inside the droplet. One notes the transition to an ordered droplet when E_0~1.4 V/nm (and ε~18) and a pronounced hysteresis as the field is decreased after the droplet has ordered. The thick dark curve derives from a fit of MD data to the Booth-Onsager equation

FIGURE 5 Droplet aspect ratios λ vs electric Bond number; predicted through the minimization of free energy with respect to λ, The two gray dashed curves are the result of using a free energy expression with no saturation term with a constant dielectric constant (top curve)and a variable dielectric constant (lower curve), neither of which correctly describes the MD results. The S-shaped region near $B_E \sim 0.25$ shows predicted metastable states (dark blue line) and stable states (lower red line), both of which are associated with an observed MD droplet state. The light blue line is where maxima of the NLPS free energy occur as the aspect ratio is varied and correspond to predicted unstable states. When a droplet is in the metastable region and the applied field is lowered to the point where the unstable region is reached the droplet aspect ratio will abruptly fall to the stable points of the lower red curve.

FIGURE 6 Comparison of the free energy F_{NLPS} (red curve) as computed by the minimization, for each E_0, of the NLPS free energy with respect to the aspect ratio and the free energy F_{MD} (blue dashed curve) computed directly from the integration of the MD total dipole moments. The two light dashed curves show the predicted free energy

for a constant and a variable dielectric constant when the free energy does not include the saturation term.

FIGURE 7 Contributions to the free energy F_{NLPS} (red curve) as computed by the minimization, for each E_0, of the NLPS free energy with respect to the aspect ratio. The same contributions (dashed lines) computed by substituting the observed MD results into the expressions for the three terms of the NLPS free energy (no minimization is involved). One can note very close agreement in all of the quantities between the MD results and the NLPS model predictions. Also shown is the close correspondence between the relative variations in surface energy and the observed relative variations in the vdW component of the internal energy. The triangles (filled for increasing E0 and empty for decreasing field) give the MD calculated VdW contribution to the internal energy.

FIGURE 8 The entropic contribution (red curve) to the free energy (green curve). The entropy increases ($-T\Delta S$ decreases) with increasing field for small droplet extensions and decreases for increasing fields after the droplet has become highly elongated. The entropy reaches a maximum in the region $E_0 \sim 0.5$-0.6 V/nm where the droplet makes a transition to a more highly elongated state.

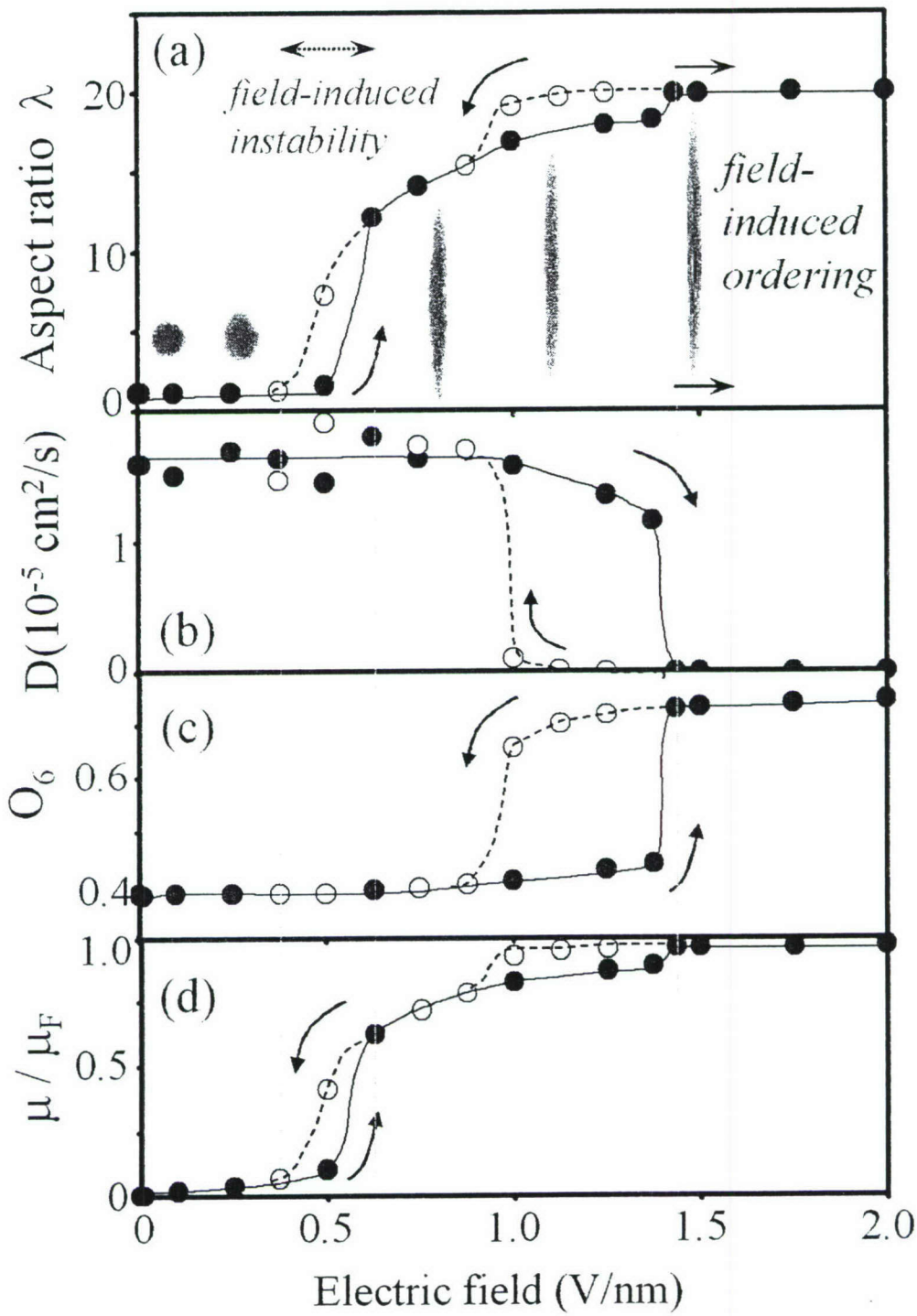
(a)
field-induced instability
field-induced ordering
Aspect ratio λ
20
10
0
(b)
D(10-5 cm2/s)
1
0
(c)
O6
0.6
0.4
(d)
μ / μF
1.0
0.5
0
0
0.5
1.0
1.5
2.0
Electric field (V/nm)

FIGURE 1

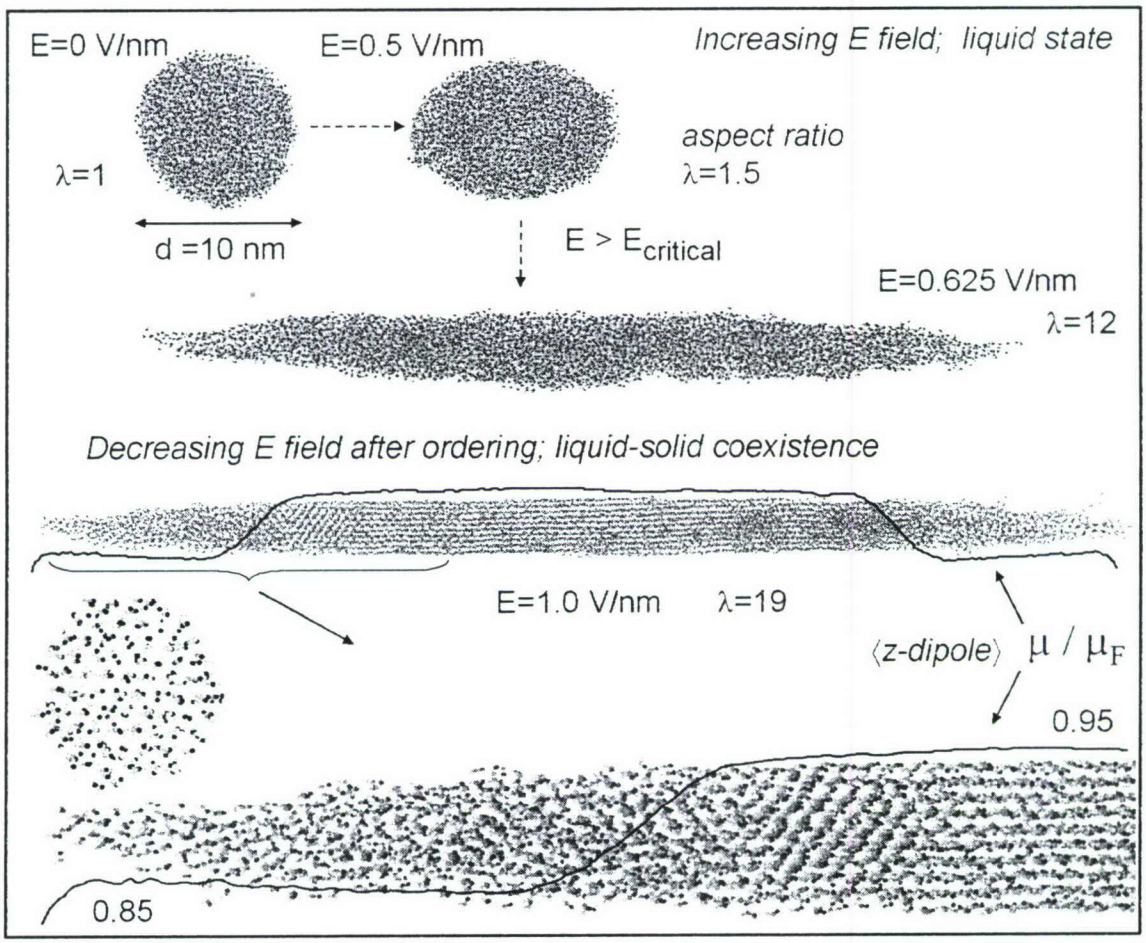
E=0 V/nm
E=0.5 V/nm
Increasing E field; liquid state
aspect ratio
λ=1.5
λ=1
d =10 nm
E > E critical
E=0.625 V/nm
λ=12
Decreasing E field after ordering; liquid-solid coexistence
E=1.0 V/nm
λ=19
⟨z-dipole⟩ μ / μF
0.95
0.85

FIGURE 2

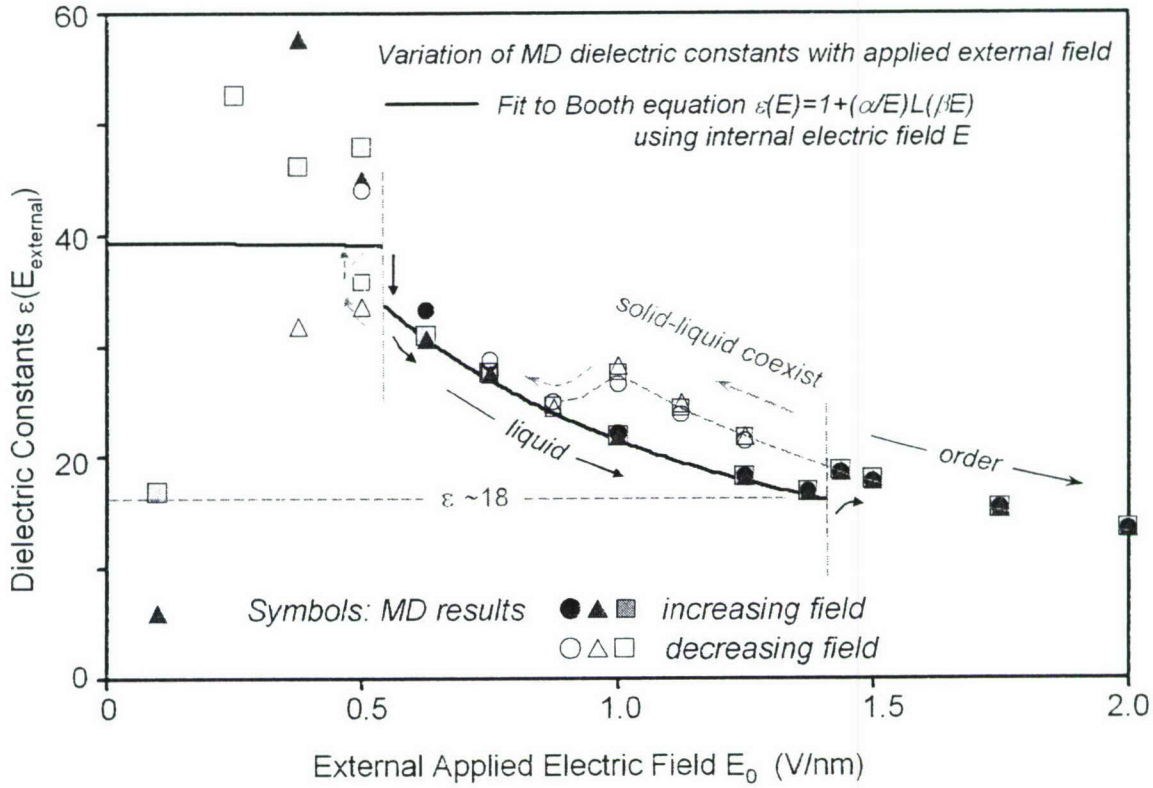
Variation of MD dielectric constants with applied external field
Fit to Booth equation ε(E)=1+(α/E)L(βE)
using internal electric field E
solid-liquid coexist
liquid
order
ε ~18
Symbols: MD results
increasing field
decreasing field
Dielectric Constants ε(E_external)
External Applied Electric Field E_0 (V/nm)
0
20
40
60
0
0.5
1.0
1.5
2.0

FIGURE 3

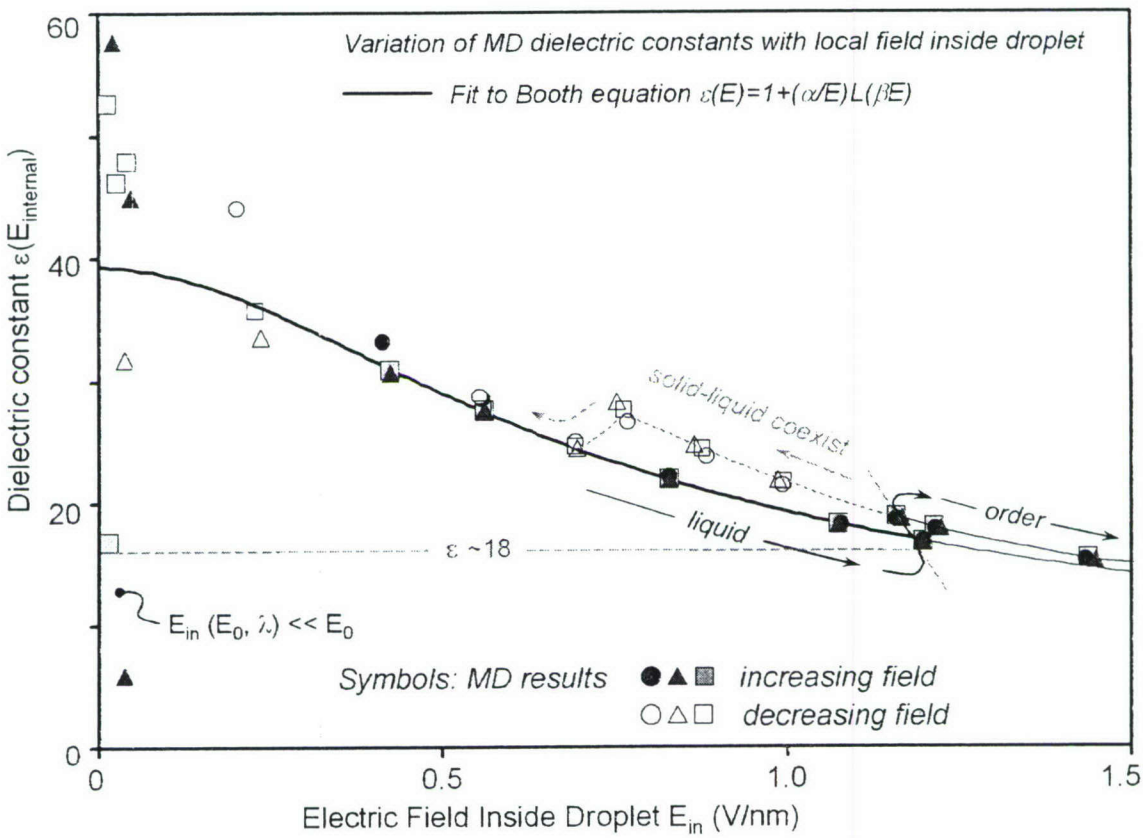
Variation of MD dielectric constants with local field inside droplet
Fit to Booth equation ε(E)=1+(α/E)L(βE)
Dielectric constant ε(E_internal)
Electric Field Inside Droplet E_in (V/nm)
solid-liquid coexist
liquid
order
ε ~18
E_in (E_0, λ) << E_0
Symbols: MD results
increasing field
decreasing field
60
40
20
0
0
0.5
1.0
1.5

FIGURE 4

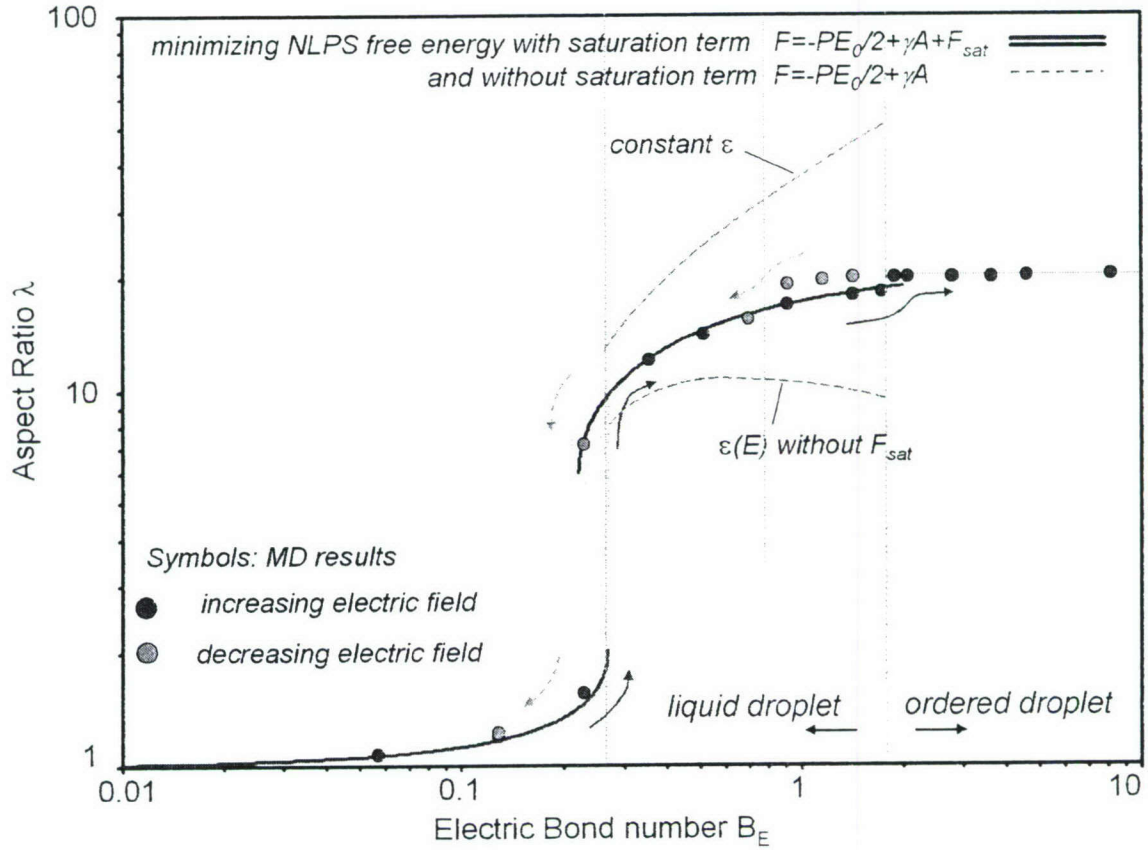
100
10
1
0.01
0.1
1
10
Aspect Ratio λ
Electric Bond number B_E
minimizing NLPS free energy with saturation term $F=-PE_0/2+\gamma A+F_{sat}$
and without saturation term $F=-PE_0/2+\gamma A$
constant ε
ε(E) without F_{sat}
Symbols: MD results
increasing electric field
decreasing electric field
liquid droplet
ordered droplet

FIGURE 5

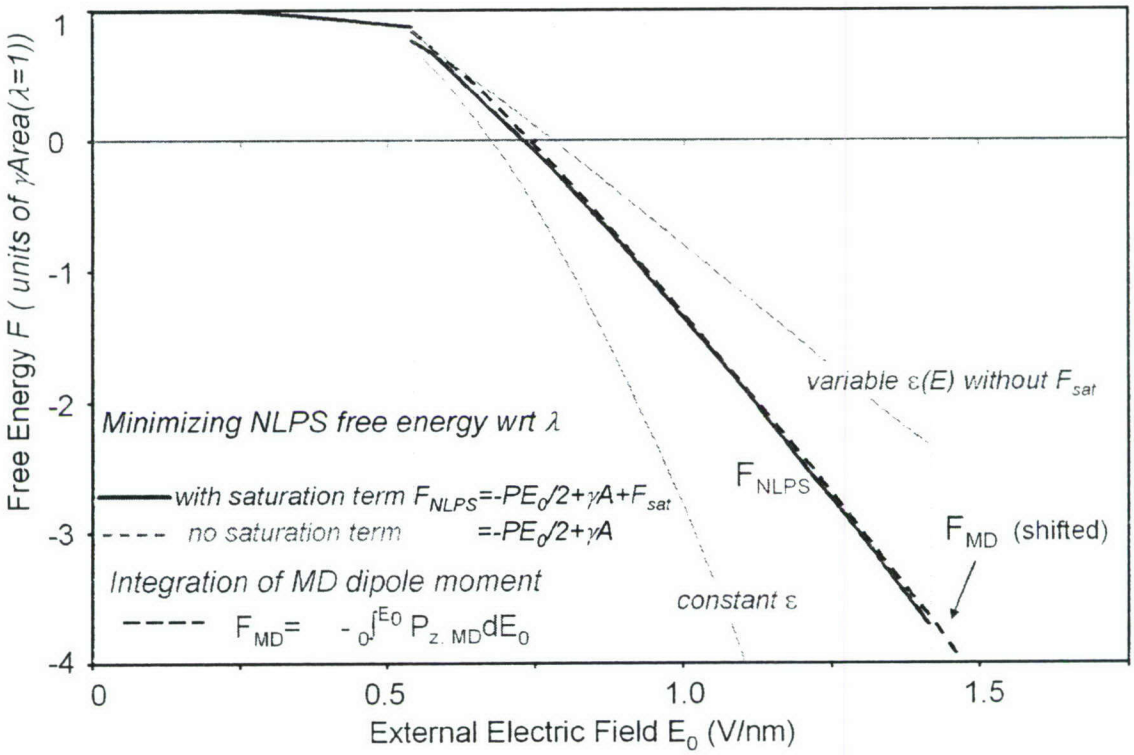
Free Energy F (units of γArea(λ=1))
External Electric Field E0 (V/nm)
1
0
-1
-2
-3
-4
0
0.5
1.0
1.5
Minimizing NLPS free energy wrt λ
with saturation term FNLPS=-PE0/2+γA+Fsat
no saturation term =-PE0/2+γA
Integration of MD dipole moment
FMD= -∫0E0 Pz. MD dE0
variable ε(E) without Fsat
FNLPS
FMD (shifted)
constant ε

FIGURE 6

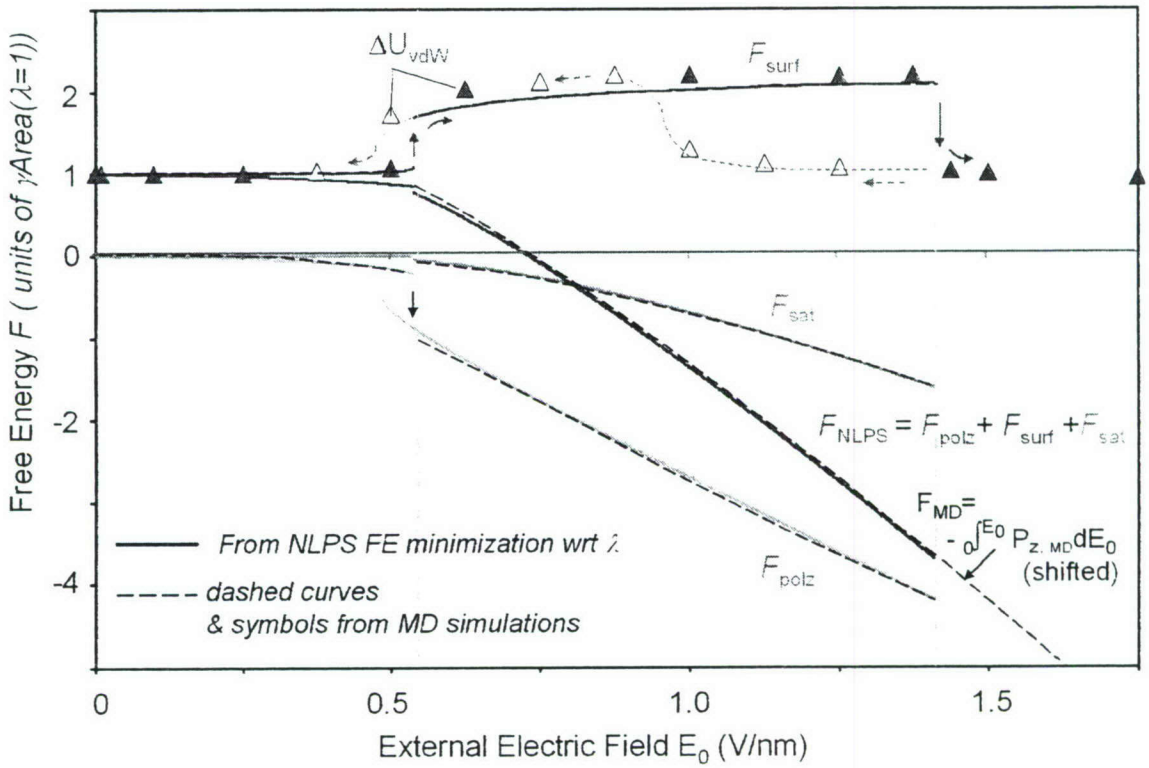
Free Energy F (units of γArea(λ=1))
External Electric Field E0 (V/nm)
ΔUvdW
Fsurf
Fsat
Fpolz
FNLPS = Fpolz + Fsurf +Fsat
FMD= - 0∫E0 Pz, MD dE0 (shifted)
From NLPS FE minimization wrt λ
dashed curves
& symbols from MD simulations
2
1
0
-2
-4
0
0.5
1.0
1.5

FIGURE 7

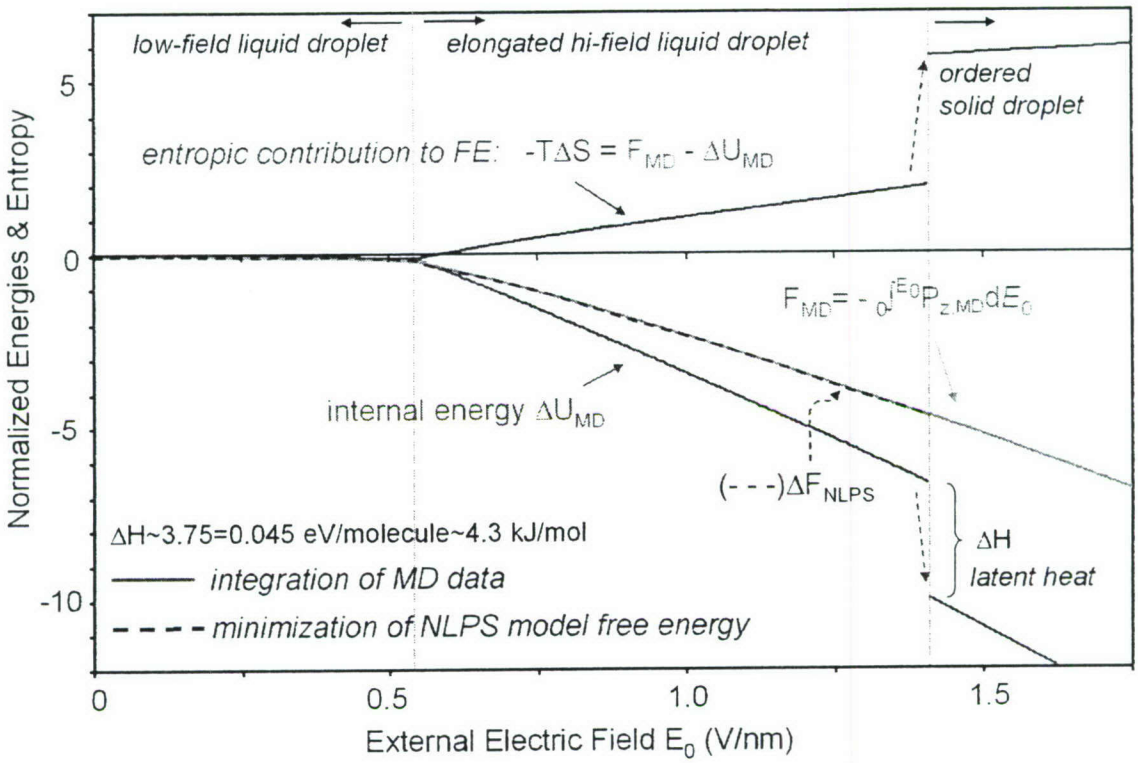
low-field liquid droplet
elongated hi-field liquid droplet
ordered
solid droplet
entropic contribution to FE: -TΔS = F_MD - ΔU_MD
F_MD = - ∫ P_z,MD dE_0
internal energy ΔU_MD
(- - -)ΔF_NLPS
ΔH
latent heat
ΔH~3.75=0.045 eV/molecule~4.3 kJ/mol
integration of MD data
minimization of NLPS model free energy
Normalized Energies & Entropy
External Electric Field E_0 (V/nm)
5
0
-5
-10
0
0.5
1.0
1.5

FIGURE 8